



**HAL**  
open science

# Application of a Broadband Active Vibration Control System to a Helicopter Trim Panel

R.H. Cabell, N.H. Schiller, F. Simon

► **To cite this version:**

R.H. Cabell, N.H. Schiller, F. Simon. Application of a Broadband Active Vibration Control System to a Helicopter Trim Panel. Noise-Con 2013, Aug 2013, DENVER, United States. hal-01058383

**HAL Id: hal-01058383**

**<https://onera.hal.science/hal-01058383>**

Submitted on 26 Aug 2014

**HAL** is a multi-disciplinary open access archive for the deposit and dissemination of scientific research documents, whether they are published or not. The documents may come from teaching and research institutions in France or abroad, or from public or private research centers.

L'archive ouverte pluridisciplinaire **HAL**, est destinée au dépôt et à la diffusion de documents scientifiques de niveau recherche, publiés ou non, émanant des établissements d'enseignement et de recherche français ou étrangers, des laboratoires publics ou privés.

## Application of a Broadband Active Vibration Control System to a Helicopter Trim Panel

Randolph H. Cabell, Noah H. Schiller	Frank Simon
NASA Langley Research Center	ONERA Centre de Toulouse
Mail Stop 463	2 Avenue Edouard Belin
Hampton, VA 23681 USA	31400 Toulouse FRANCE
randolph.h.cabell@nasa.gov	

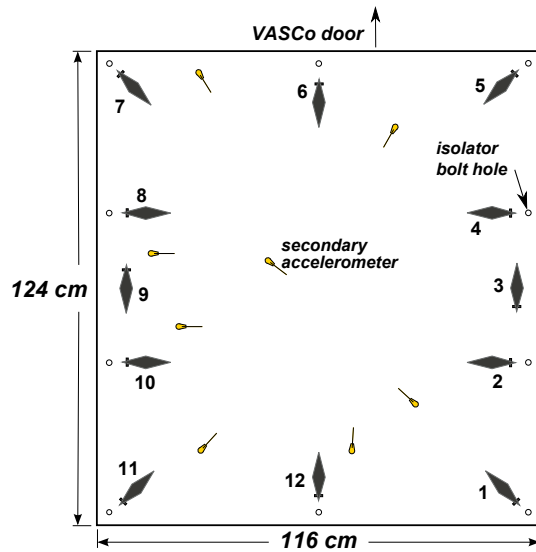
### ABSTRACT

This paper discusses testing of a broadband active vibration control concept on an interior trim panel in a helicopter cabin mockup located at ONERA's Centre de Toulouse. The control system consisted of twelve diamond-shaped piezoelectric actuators distributed around a 1.2m x 1.2m trim panel. Accelerometers were mounted at the four vertices of each diamond. The aspect ratio of the diamond was based on the dielectric constants of the piezoelectric material in order to create an actuator-sensor pair that was collocated over a broad frequency range. This allowed robust control to be implemented using simple, low power analog electronics. Initial testing on a thick acrylic window demonstrated the capability of the controller, but actuator performance was less satisfactory when mounted on a composite sandwich trim panel. This may have been due to the orthotropic nature of the trim panel, or due to its much higher stiffness relative to the acrylic window. Insights gained from a finite element study of the actuator-sensor-structural system are discussed.

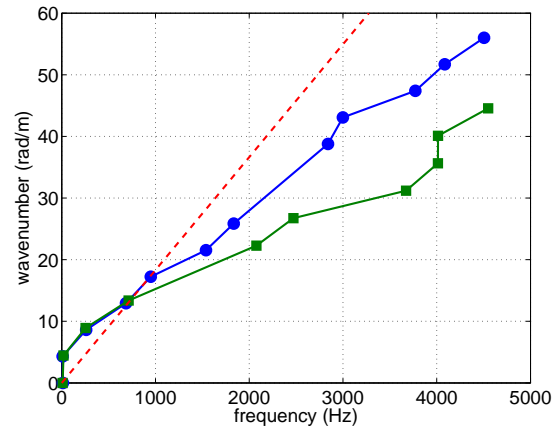
### 1. Introduction

Helicopter interior noise levels have long been recognized as adversely affecting passenger and crew comfort. The problem is partly due to the proximity of powertrain components, such as the main rotor transmission, hydraulic pumps, and the engine, to the passenger compartment. These excitation sources create vibrational energy that is readily distributed throughout a lightweight, structurally efficient airframe, and then re-radiates into the passenger cabin as offending noise. Numerous references can be found describing work conducted over the past four decades to study and reduce noise levels inside helicopters [1, 2, 3, 4, 5, 6]. The difficulty of the problem is compounded by the extreme weight sensitivity of helicopters, so any noise reduction technology must be lightweight. Given the tightly coupled nature of the mechanical sources, the airframe, and the passenger cabin, a system-level solution that addresses the source, the propagation path, and radiation of energy into the cabin acoustic volume is likely to be necessary.

The approach described in this paper represents a technology for the radiation part of the interior noise problem. Specifically, this paper describes a compact, lightweight actuator-sensor combination that actively adds damping to a structure. The technology could be applied to a sidewall or trim panel that receives mechanical energy that is then re-radiated as sound into the passenger cabin. Because the approach actively adds damping to a structure, it can be used to reduce sound radiation from panels excited above their acoustic coincidence frequency. An example of such a structure is a lightweight, stiff interior trim panel driven by high frequency energy from the helicopter's powertrain.



(a) Trim panel dimensions and actuator layout.



(b) Estimated dispersion (blue circles-horiz., green squares-vert., dashed red-acoustic)

Figure 1: Panel.

The control approach is based on a piezoelectric transducer with a highly directional strain response created by inter-digitated electrodes on the transducer. These electrodes apply the electric field in the plane of the actuator rather than through the actuator's thickness, as found on many other piezoelectric devices. A procedure described previously [7] specifies how to compute the aspect ratio of a diamond-shaped actuator based on the dielectric constants of the actuator material in order to minimize moments generated by the actuator. The resulting diamond actuator effectively couples as four point forces to the structure, thereby enabling simple velocity feedback control to be implemented using analog electronic circuitry. Earlier benchtop testing of the approach on an acrylic panel successfully demonstrated broadband vibration reduction [7].

The test described in this paper was used to demonstrate the control approach on a more complex structure. Specifically, twelve actuators were applied to a lightweight sandwich structure representing a non-load bearing trim panel in a helicopter cabin. The panel was mounted to the roof of a helicopter cabin mockup located at ONERA's Centre de Toulouse. A roof beam of the cabin mockup was externally excited by a shaker to simulate mechanical input from the powertrain. Reductions in the panel vibration and cabin noise levels were measured.

This document summarizes the control approach and test results, but also discusses performance issues with the actuator that were discovered during testing. Preliminary conclusions from a finite element analysis of the control system are discussed to motivate future work to improve the performance.

## 2. Equipment

### A. Trim Panel

A rectangular, composite sandwich trim panel was fabricated with dimensions shown in figure 1(a). The facesheets of the sandwich structure consisted of four plies of unidirectional carbon/epoxy with ply angles of:  $0^\circ/90^\circ/90^\circ/0^\circ$ , where  $0^\circ$  corresponds to the long dimension of the trim panel. After curing, the facesheets were secondarily bonded to a 1.91 cm-thick honeycomb core using an adhesive film and vacuum bag pressure.

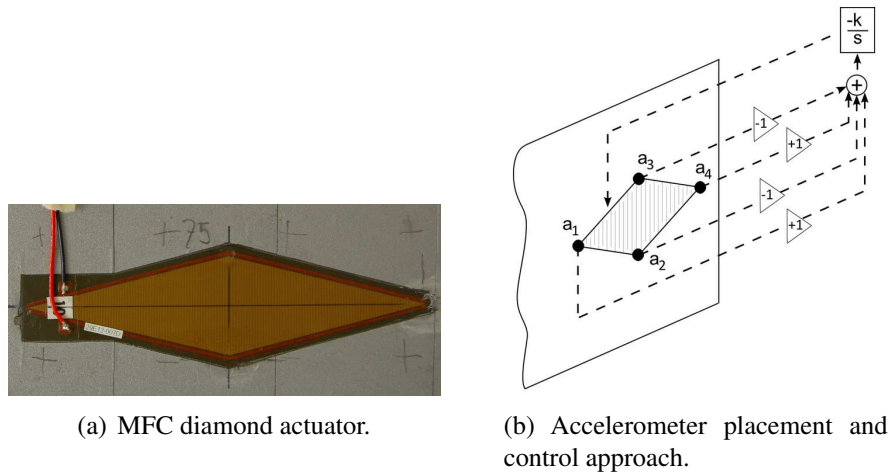


Figure 2: MFC Actuator.

The experimentally estimated dispersion characteristics of the panel are shown in figure 1(b). These values were estimated by Fourier decomposition of horizontal and vertical scans of the panel using a laser vibrometer while the panel was suspended vertically and excited by a shaker. The difference between the horizontal and vertical dispersion reflects the orthotropic nature of the panel. The crossover between the acoustic wavenumber, in red, and the flexural wavenumbers indicates the coincidence frequencies of this panel, where the acoustic transmission loss is low.

## B. Actuators, Sensors, and Control Circuits

The control actuators were P1 type macro-fiber composites (MFCs), which are piezoelectric patch actuators with inter-digitated electrodes that apply the electric field in an in-plane direction. A photo of the actuator mounted on the trim panel is shown in figure 2(a). The inter-digitated electrodes appear in the photograph as a series of closely-spaced vertical lines. The actuator's dimensions are approximately 12.7 cm by 3.2 cm. The aspect ratio of the diamond was specified based on the material properties of the actuator, including the two in-plane dielectric constants, to minimize the edge moments generated by the actuator. With this design approach, the resulting net effect of the actuator on the structure, in the ideal case, reduces to four point forces acting at each of the four actuator vertices [7]. The two point forces created at the left and right actuator vertices in the photo are  $180^\circ$  out of phase with the two point forces at the top and bottom vertices.

By placing accelerometers at the four vertices, integrating their outputs, and summing as indicated in figure 2(b), a matched force-velocity transducer is created. A matched actuator-transducer pair enables robust, broadband feedback control to be applied using simple analog electronics. For the work described here, lightweight (0.4 g) accelerometers were mounted at the vertices of each actuator. The same model accelerometers were also used for secondary sensing at the locations shown in figure 1(a) to quantify the vibration of the trim panel.

Twelve actuators were distributed around the trim panel as shown in figure 1(a). The actuators were placed near points where the panel was attached to the roof of the test structure via vibration isolators. Although the actuators could have been placed using an optimization scheme, it seemed unlikely that such a scheme would produce a dramatic enough improvement in performance to justify the complexity of modeling the panel, excitation, actuators, and dealing with the uncertainties in the dynamics of each of these items.

Although the feedback control scheme implemented here is effective over a very wide frequency bandwidth, the authority of the actuator depends on the relative size of the actuator compared to the flexural

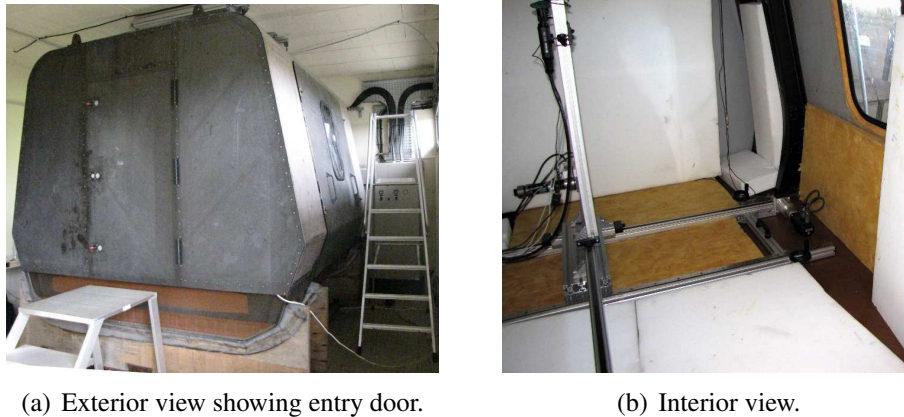


Figure 3: VASCo (helicopter cabin mockup).

wavelengths in the trim panel. The nominal dimensions of the actuator were chosen in order to couple effectively into flexural waves between 1 and 2 kHz, based on a finite element model of the trim panel.

Due to the simplicity of the control algorithm, it was possible to build the control circuits using only analog electronics [7]. Each control circuit contained signal conditioning for the accelerometers, control logic, and amplification for the actuator drive signal. The transfer function relating the output voltage,  $Y$ , to an accelerometer input,  $X$ , is given by

$$\frac{Y(j\omega)}{X(j\omega)} = 42700 \frac{jK}{f}$$

where  $f$  is frequency (Hz) and  $K$  is the adjustable circuit gain, from 10 to 60. The actual transfer function varied from the above equation at very low frequencies due to decoupling capacitors and at very high frequencies due to limitations of the operational amplifiers.

All control circuits were powered by a single step-up circuit board that converted a 28 VDC input to 96 VDC. The control authority of the piezoelectric actuators roughly scales with input voltage, so the 96 VDC voltage was specified to ensure sufficient actuation authority to control moderate excitations of the panel.

### C. Helicopter Cabin Mockup: VASCo

VASCo, or Vibro-Acoustique de Structures Composites, is a full-scale section of a helicopter cabin constructed for ONERA Centre de Toulouse by Eurocopter to test cabin noise reduction concepts [8]. The structure consists of composite stiffeners and composite sandwich sidewalls with two acrylic windows and a plywood floor. A door in one end provides access to the interior. Exterior and interior photos of VASCo are shown in figure 3. The interior photo shows pieces of foam and fiberglass in the cabin that were used to de-reverberate the space during testing. A traversing rig that supported a laser vibrometer is also visible in the interior photo.

The trim panel was attached to the roof beams in VASCo via ten vibration isolators around the perimeter of the panel. Disturbance excitation was provided by an electrodynamic shaker attached to the exterior roof of VASCo, at the intersection of two roof support beams. This was done to approximate mechanical excitation from a powertrain component, such as the main transmission, in close proximity to the passenger cabin. The shaker was driven with a broadband signal with an approximately flat spectral response ( $\pm 1$  dB) from 100 Hz to 20000 Hz. In order to reduce acoustic excitation of the trim panel and the influence of

acoustic resonances of the space immediately above the trim panel, a piece of melamine foam approximately 7 cm thick was positioned above the panel in the space created by the depth of the VASCo stiffeners. The foam was supported by the flanges of the stiffeners and was not touching the trim panel.

### 3. Results

The performance of the control system is discussed here in terms of the trim panel velocity as measured at eight secondary accelerometers, shown in figure 1(a). Comparisons are made between the accelerometer responses with the control actuators unpowered and powered. Although additional measurements were made during testing, including the trim panel velocity measured with a scanning laser vibrometer, and sound intensity at a dense grid of measurement points just off the surface of the trim panel, only secondary accelerometer response is discussed here. These accelerometer responses are sufficient to convey the performance of the control system, and they had the lowest uncertainty of the measurements made.

During tuning of the control system gains, after the trim panel had been mounted in VASCo, it was observed that the feedback gain of all of the control circuits had to be greatly reduced to avoid an instability near 10 kHz. Although the specific frequency of instability varied, the frequency responses of all the circuits contained an unexpected phase rolloff below 10 kHz. While some phase rolloff is to be expected at high frequencies, this rolloff occurred at a much lower frequency than expected, where the actuator still had a high degree of coupling with the structure. The gain reduction needed to maintain stability had the unfortunate side effect of reducing the control performance of each circuit.

Frequency responses from the input to the shaker to the eight secondary accelerometer responses were measured in order to quantify control system performance. The performance metric was defined as

$$Y(\omega) = 10 \log_{10} \left( \frac{\mathbf{V}_{\text{off}}^2(\omega)}{\mathbf{V}_{\text{on}}^2(\omega)} \right) \quad (1)$$

where  $\mathbf{V}_{\text{off}}^2$  denotes the sum of the squared velocity responses of the secondary accelerometers with the control system off, and  $\mathbf{V}_{\text{on}}^2$  is the same quantity with the control system on. A positive value of the metric,  $Y$ , indicates the velocity response of the panel was lower with the control system turned on than when it was off. The quantity  $\mathbf{V}^2$  was computed as

$$\mathbf{V}^2(\omega) = \sum_{i=1}^8 G_{vvi}(\omega) \quad (2)$$

where  $G_{vvi}(\omega)$  is the power spectrum of the velocity response at the  $i$ th secondary accelerometer.

Values of the metric in Eq. 1 for the broadband shaker excitation case are shown in figure 4. Results are averaged over third-octave bands, with two standard deviations about the average indicated by the red bars. The standard deviation was computed using a propagation of error approach [9], and is largely determined by the coherence and number of averages used in computing the frequency responses of the secondary accelerometers. Poor coherence is generally due to either the drive signal amplitude being very small or the excitation coupling poorly to the trim panel response (below  $\approx 500$  Hz).

The results indicate that the control system did very little to attenuate panel vibration. The lower uncertainty bound in figure 4 exceeded 0 dB only from 1250 Hz to 3150 Hz, while the average reduction in these bands ranged from 0.2 dB to 0.4 dB. Hence, only in these five 1/3-octave bands can it be said with some confidence that the control system reduced the panel response. Likewise, the upper uncertainty bound was less than zero, indicating the controller increased the panel vibration, in the 5, 8, and 10 kHz third-octave bands. The control system was not expected to have spillover, or an increase in panel response when turned on, in the ideal case. This increased response could have been due to the controller instabilities noticed while tuning the controller gains.

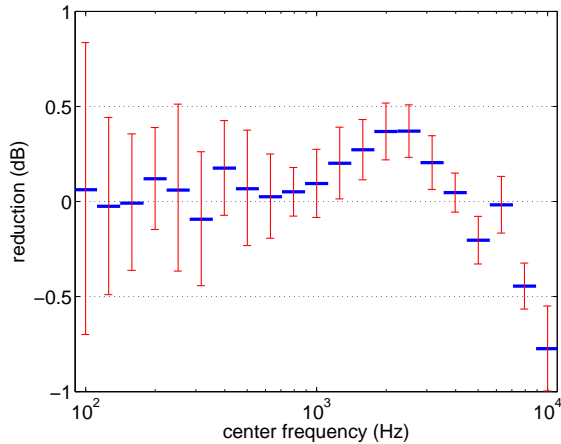


Figure 4: Reduction,  $Y$  (eq. 1), of secondary accelerometer responses produced by the control system.

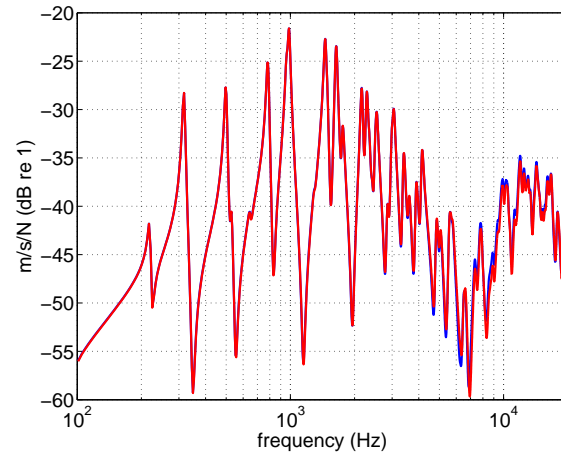


Figure 5: Comparison of FRFs from FE model. Blue - 4 point forces at actuator vertices. Red - thermal input to actuator.

#### 4. Discussion

Robust performance of the control system assumes the diamond-shaped piezoelectric actuator couples to the structure in the same way as four point forces at the diamond's vertices. The aspect ratio of the diamond was specified to ensure this condition would be met. However, when this assumption is inaccurate, the actuator-accelerometer arrangement deviates from a collocated force-velocity system. As a result, a control system based on simple velocity feedback may add energy to the system, or even go unstable, rather than adding damping. The poor performance of the diamond actuators on the composite sandwich panel, and specifically, the fact that the feedback gain had to be substantially reduced in order to keep the control system stable, suggests the actuator-accelerometer arrangement was not collocated, and hence the point-force assumption was invalid.

To explore the validity of the point force assumption on different types of structures, a finite element (FE) model of a diamond actuator on a plate was created. This model used a thermal analogy [10] to simulate the response of the structure to a strain actuator such as the piezoelectric one applied here. With this analogy, thermal expansion coefficients of the piezoelectric material are specified based on the actual dielectric coefficients of the piezoelectric material (the strain-charge, or  $d_{ij}$ , values). A periodically varying temperature was then applied to the piezoelectric material in the FE model. The resulting thermal strain in the actuator coupled to the structure and created a structural response similar to the response created when a periodically varying electric field was applied to the actuator.

Three different base structures were studied using the finite element models: a thin steel plate, a composite laminate facesheet, and a sandwich panel representing the trim panel used in the VASCo test. The steel plate was 2.3 mm thick, while the facesheet laminate consisted of 4 layers of carbon fiber, with a total thickness of 0.5 mm. All plies in the laminate were at  $0^\circ$  relative to the long axis of the diamond actuator. In all cases the structures and actuator-structure combinations were modeled using 2D shell elements and the PCOMP card in NASTRAN, which specifies laminates of multiple materials [11].

Frequency responses from thermal and point force inputs to velocity responses at the actuator vertices were computed and compared. In all cases the velocities at the actuator vertices were summed as indicated in figure 2(b). For the point-force excitation, the applied point forces at the vertices were also phased as shown in figure 2(b), such that the forces applied at the vertices labeled  $a_1$  and  $a_4$  had the same phase as one another but were oppositely phased from the forces applied to the vertices labeled  $a_2$  and  $a_3$ . The actuator was included in the force FE models as a passive structural element, thus accounting for its mass

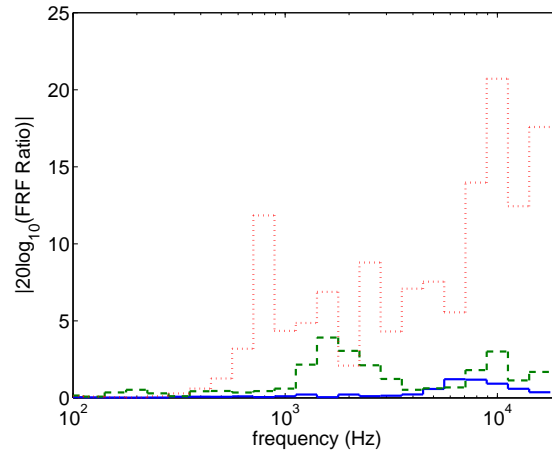


Figure 6: Agreement between force and thermal FRFs. Blue solid line -steel plate; Green dashed line-0°-laminated; Red dotted line-sandwich panel.

and stiffness effects.

Figure 5 shows an example comparison of force and thermal FRFs for the actuator on the steel plate. The two FRFs show excellent agreement over nearly the entire analysis frequency range. The agreement between FRF magnitudes was quantified using the following metric:

$$W = \left\langle \left| 20 \log_{10} \frac{|\text{FRF}_{\text{force}}|}{|\text{FRF}_{\text{thermal}}|} \right| \right\rangle_{1/3 \text{ octave}} \quad (3)$$

This is essentially an average over 1/3-octave bands of the absolute value of the dB deviations between the two FRFs. While the phase relationship between the two FRFs is also important, the  $W$  metric provides a succinct summary of the agreement for this study.

Values of the metric,  $W$ , are shown in figure 6 for the diamond actuator on the three structures. A low value of the metric indicates good agreement between the force and thermal FRFs, and hence suggests the point-force representation of the diamond actuator is accurate. Note that the blue curve in the figure quantifies the agreement between the force and thermal FRFs shown in figure 5. The low values of the blue curve reflect the close agreement between the force and thermal FRF magnitudes for the actuator on the steel plate, especially below 2 kHz. Some small differences between the FRFs occur above that frequency. In contrast, the green and red curves reflect larger discrepancies between the force and thermal FRFs for the 0°-laminated and especially the sandwich panel.

While this finite element analysis doesn't yet answer the question of exactly why the actuator performance was disappointing in the ONERA test, the analysis does suggest an area for further exploration. Specifically, the point-force representation of the diamond actuator appears to be invalid when the actuator is mounted on an orthotropic facesheet or on a more complicated, orthotropic sandwich panel. This finite element model, coupled with a more fundamental analysis of a piezoelectrically coupled electromechanical system [12], will hopefully yield design guidelines that enable application of the control approach to non-isotropic structures.

## 5. Conclusions

A control system designed to produce robust, broadband damping was tested on a composite sandwich trim panel mounted in a helicopter cabin mockup. The control system consisted of twelve piezoelectric diamond actuators with an accelerometer attached to each vertex of each actuator. The geometry and material properties of the actuator enabled simple velocity feedback to be implemented using analog circuitry. Although

the control approach had been tested previously and performed well on an isotropic panel, performance was not as good on the composite panel since feedback gains had to be greatly reduced to maintain controller stability. As a result of this gain reduction, the controllers produced only modest reductions ( $<0.5$  dB) in the velocity of the trim panel between 1 and 3 kHz when the exterior of the helicopter cabin was excited by a shaker. Results from a finite element study of the actuator applied to a range of structures suggest the optimal geometry of the actuator that enables collocated feedback control may depend on the orthotropic nature of the underlying structure, and warrants further study.

## REFERENCES

- [1] John J. Sciarra, Robert W. Howells, and Jr. Joseph W. Lenski. Helicopter transmission vibration and noise reduction program. Technical Report USARTL-TR-78-2A (ADA055104), US Army Research and Technology Laboratories, 1978.
- [2] C.A. Yoerkie, P.J. Gintoli, S.T. Ingraham, and J.A. Moore. Development of rotorcraft interior noise control concepts: Phase III: Development of noise control concepts. Technical Report CR-178172, NASA, 1987.
- [3] Thomas A. Millott, William A. Welsh, Charles A. Yoerkie, Jr., Douglas G. MacMartin, and Mark W. Davis. Flight test of active gear-mesh noise control on the S-76 aircraft. In *Proceedings of the 54th Annual Forum of the American Helicopter Society*, Washington, D.C., May 1998.
- [4] Pierre Belanger, Alain Berry, Yann Pasco, Olivier Robin, Yves St-Amant, and Srivatsa Rajan. Multi-harmonic active structural acoustic control of a helicopter main transmission noise using the principal component analysis. *Applied Acoustics*, 70:153–164, 2009.
- [5] F. Simon and S. Pauzin. Active vibration control procedure to reduce internal noise of helicopter cabin. In *American Helicopter Society Technical Specialists' Meeting for Rotorcraft Acoustics and Aerodynamics*, Williamsburg, Virginia, October 1997.
- [6] F. Simon and S. Pauzin. Adaptive active experiment to reduce multi-tonal noise in a generic composite helicopter cabin. In *Proceedings of the 26th European Rotorcraft Forum*, The Hague, September 2000.
- [7] Noah H. Schiller, Daniel F. Perey, and Randolph H. Cabell. Development of a practical broadband active vibration control system. In *Proceedings of the ASME 2011 International Mechanical Engineering Congress & Exposition, IMECE2011*, Denver, Colorado, 2011.
- [8] G. Martin, F. Simon, and D. Biron. Detection of acoustic radiating areas of a generic helicopter cabin by beamforming. In *155th Meeting of the Acoustical Society of America*, Paris, France, July 2008.
- [9] H.H. Ku. Notes on the use of propagation of error formulas. *Journal of Research of the National Bureau of Standards - C. Engineering and Instrumentation*, 70C(4):263–273, Oct-Dec 1966.
- [10] F. Côté, P. Masson, N. Mrad, and V. Cotoni. Dynamic and static modelling of piezoelectric composite structures using a thermal analogy with MSC/NASTRAN. *Composite Structures*, 65:471–484, 2004.
- [11] MSC Software Corporation, Santa Ana, CA. *MSC Nastran 2007 r1: Release Guide*, 2007.
- [12] Nesbitt W. Hagood, Walter H. Chung, and Andreas von Flotow. Modelling of piezoelectric actuator dynamics for active structural control. In *31st Structures, Structural Dynamics and Materials Conference*, number AIAA 90-1087, 1990.